JAMES | Journal of Advances in Modeling Earth Systems

RESEARCH ARTICLE
10.1029/2020MS002187

Impacts of Assimilation Frequency on Ensemble Kalman Filter Data Assimilation and Imbalances

Huan He[1], Lili Lei[1,2], Jeffrey S. Whitaker[3], and Zhe-Min Tan[1]

[1]Key Laboratory of Mesoscale Severe Weather, Ministry of Education, Nanjing University, Nanjing, China, [2]School of Atmospheric Sciences, Nanjing University, Nanjing, China, [3]NOAA/Earth System Research Laboratory/Physical Sciences Division, Boulder, CO, USA

Key Points:
- Increasing assimilation frequency can reduce errors for state variables that are not sensitive to imbalances
- For variables sensitive to imbalances, increasing assimilation frequency without IAU results in less insertion noises and reduced errors
- Increasing assimilation frequency with IAU has lessened noise filtering and increases errors for state variables sensitive to imbalances

Correspondence to:
L. Lei,
lililei@nju.edu.cn

Citation:
He, H., Lei, L., Whitaker, J. S., & Tan, Z.-M. (2020). Impacts of assimilation frequency on ensemble Kalman filter data assimilation and imbalances. *Journal of Advances in Modeling Earth Systems*, *12*, e2020MS002187. https://doi.org/10.1029/2020MS002187

Received 21 MAY 2020
Accepted 6 OCT 2020
Accepted article online 12 OCT 2020

Abstract The ensemble Kalman filter (EnKF) has been widely used in atmosphere, ocean, and land applications. The observing network has been significantly developed, and thus, observations with highly dense temporal resolutions have become available. To better extract information from dense temporal observations, one straightforward strategy is to increase the assimilation frequency. However, more frequent assimilation may exacerbate the model imbalance and result in degraded forecasts. To combat the imbalance caused by ensemble-based data assimilation due to sampling error and covariance localization, three- and four-dimensional incremental analysis update (IAU) were proposed, which gradually introduce the analysis increments into model rather than intermittently updating the state. The trade-off between the assimilation frequency and imbalance is systematically explored here by using an idealized two-layer model and the NOAA GFS. Results from the idealized two-layer model show that increasing assimilation frequency can reduce errors for state variables that are not sensitive to imbalances. For state variable that carries the signal of the external gravity mode and is sensitive to imbalances, increasing assimilation frequency without (with) IAU reduces (increases) errors. Without IAU, more frequent updates result in smaller increments and less insertion noise, while the initialization of IAU cannot effectively mitigate the imbalances with increased assimilation frequency. Results with a low-resolution version of the NOAA GFS demonstrate that increasing assimilation frequency from 6 to 2 h improves the errors and biases of forecasts verified with conventional and radiance observations, although gravity wave noise in the forecast is increased.

Plain Language Summary Data assimilation combines observations with prior information like model forecasts to produce the best estimate of the state for a dynamical system. For global prediction, a data assimilation interval of 6-h has typically been used; but for high-resolution regional models with dense spatial and temporal resolution observations such as radar and satellite data, shorter data assimilation intervals are often used. Given the significantly developed observing networks, observations with highly dense temporal resolutions and inhomogeneous spatial distributions have become available. Increasing the assimilation frequency may better extract information from dense temporal observations, but does not give the model enough time to adjust the updated state variables with potentially insertion shocks. This study systematically investigates the trade-off between the data assimilation frequency and imbalance. Results reveal that increasing assimilation frequency can reduce errors for state variables, because more frequent updates can better fit the model to the observation and result in smaller increments/less imbalances to the model. When the incremental analysis update (IAU) is applied, increasing assimilation frequency reduces errors for state variables that are not sensitive to imbalances, but the opposite for state variables sensitive to imbalances, because the IAU with more frequent assimilation cannot effectively mitigate the imbalances.

1. Introduction

Data assimilation (DA) combines observations with prior information like model forecasts to produce the best estimate of the state for a dynamical system (e.g., Kalnay, 2002). DA approaches have been widely used for numerical weather prediction. For global prediction, a DA interval of 6-h has typically been used (e.g., Buehner et al., 2010a, 2010b; Houtekamer & Mitchell, 2005; Houtekamer et al., 2014; Whitaker et al., 2008).

In contrast, high-resolution regional models with dense spatial and temporal resolution observations such as radar and satellite data often use shorter DA intervals (e.g., Aksoy et al., 2009; Honda et al., 2018; Snyder & Zhang, 2003). For assimilation of radar data on the convective scale, Hu and Xue (2007) used a three-dimensional variational (3DVAR; Gao et al., 2004) method to assimilate radar data for a tornadic thunderstorm case, and found that 10-min DA intervals led to better storm predictions compared to 5- and 15-min intervals. Pan and Wang (2019) showed that 20-min DA intervals produced better forecasts of a squall line system. Using an ensemble Kalman filter (EnKF; Whitaker & Hamill, 2002; Johnson et al., 2015) to assimilate radar data, Johnson and Wang (2017) suggested that 10-min DA intervals led to more skillful convective precipitation forecasts than both shorter and longer intervals. For simulation and prediction of hurricane Ike (2008), Dong and Xue (2013) showed that 30-min DA intervals produced results similar to 10-min intervals, while 60-min intervals were too long.

Lei and Anderson (2014) investigated the impacts of frequently assimilating only surface pressure observations. Results showed that by observing only surface pressure, the uncertainty throughout the entire depth of the troposphere can be constrained, and the analysis error over the entire depth of the troposphere was reduced with increased assimilation frequency. Similarly, Penny et al. (2019) found that with high-frequency analysis update and with large ensemble size, assimilating only ocean observations could generate ocean analyses that are almost as accurate as when assimilating both atmosphere and ocean observations. As the assimilation frequency decreases, accuracy from assimilating only ocean observations decreased relative to assimilating all observations.

Different DA intervals have also been applied into other geophysical applications. Valdes-Abellan et al. (2019) studied the impact of assimilation frequency of water content measurements for obtaining soil hydraulic parameters. Using an EnKF with a state augmentation approach to update both model states and parameters, results showed that high frequency update does not provide better soil hydraulic parameters than low frequency update. Lawson et al. (1996) explored the impact of assimilation frequency on recovery of rate parameters for a simple marine ecosystem. Their results suggested that increasing the data availability from bi-weekly to weekly intervals did not significantly improve the parameters, and concluded that recovery of component initial conditions was related to the timescale of the biological processes and more frequent data were required for faster processes.

Previous studies have shown that frequency of measurements and updates are important for DA. Some studies suggest that more frequent assimilation can lead to better results. Given the significantly developed observing networks, observations with highly dense temporal resolutions and inhomogeneous spatial distributions like the satellite radiances have become available. To better extract information from dense temporal observations, one straightforward strategy is to increase the assimilation frequency. However, too frequent of an interval does not give the model enough time to adjust to the increments, and frequent stopping and restarting of the model with intermittent DA updates can potentially introduce imbalances and result in insertion noise in numerical models (e.g., Lei et al., 2012b; Wang et al., 2013). The insertion noise is often caused by intermittent DA, since the model state is updated at every assimilation time when an analysis is performed (Lei et al., 2012a). Several strategies to combat the imbalance in the intermittent DA have been developed, including the normal mode initialization (Baer & Tribbia, 1977; Machenhauer, 1977), digital filtering (DFI; Lynch & Huang, 1992; Huang & Lynch, 1993), and incremental analysis update (IAU; Bloom et al., 1996; Lei & Whitaker, 2016). On the other hand, using longer DA intervals can avoid imbalances due to frequent updates, but with longer DA intervals, the linear and Gaussian assumptions of DA methods (e.g., 3DVAR and EnKF) tend to be violated with more nonlinear perturbation growth in the longer forecasts.

Although the DA frequency has strong effects on DA performance, studies that provide guidance on the appropriate DA frequency for different applications are rare. Therefore, the trade-off between the DA frequency and imbalance is investigated in this study. Using an idealized two-layer primitive equation model, the impacts of assimilation frequency and imbalance and the impact of initialization methods such as the three-dimensional IAU (3DIAU; Bloom et al., 1996) and four-dimensional IAU (4DIAU; Lei & Whitaker, 2016) are systematically examined. To assess the relevance of this simplified framework, we also perform experiments with a low-resolution version of the previous generation of the operational NOAA Global Forecast System (GFS) using a 2-h (rather than a 6-h) DA interval.

The structure of this paper is as follows. Section 2 describes the two-layer model and experimental design. The results from the two-layer model are discussed in section 3. The design of experiments with the NOAA GFS is explained in section 4, and results from the GFS experiments are presented in section 5. The conclusions are summarized in section 6.

2. Design of the Two-Layer Model Experiments

2.1. Two-Layer Model

To examine the impact of assimilation frequency, a dry, global, two-layer primitive-equation model is used (Zou et al., 1993). This model consists of two layers of constant potential temperature on a rotating sphere. The upper boundary is assumed to be a free surface, and the dynamics of each layer is similar to that of a shallow-water model. The two-layer model is spectral and is run at triangular truncation of T32. The model state vector consists of vorticity and divergence spectral coefficients at two levels and coefficients of layer thickness as Exner function at the lower surface and at the interface. This model was used for ensemble data assimilation and initialization experiments (e.g., Hamill & Whitaker, 2005; Lei & Whitaker, 2016).

Configuration of the two-layer model follows Hamill and Whitaker (2005) and Lei and Whitaker (2016). A zonal wavenumber-2 terrain with a maximum (minimum) amplitude of 2,000 (−2,000) m at latitudes of 45°N and 45°S and longitudes of 0° and 180° (90° and 270°) is imposed, whose amplitudes smoothly decrease to 0 m at the poles and equator. The model is forced by Newtonian relaxation to a prescribed interface Exner function with a damping time scale of 20 days. The surface Exner function is diagnosed by the summation of the fixed Exner function at model top and thickness of the two layers. There is ∇^8 hyperdiffusion with a 12-h e-folding time scale for the shortest resolvable scale. A fourth-order Runge-Kutta scheme is used for numerical integration, and the time step is 15 min. The error-doubling time of the model at T32 is approximately 4 days.

2.2. OSSE

Using the two-layer model, observing system simulation experiments (OSSEs) are conducted. Model resolution T32 is used for a nature run and all simulation experiments, so that these are "perfect model" or "identical twin" experiments. Synthetic observations of interface pseudo-height (true height in an isentropic atmosphere, unit: m) are generated by adding random errors with distribution of $N(0, \sqrt{1{,}000})$ m to spatially interpolated values from the nature run. The observation error variance (1,000) is about 1% of the globally averaged climatological variance in the natural run. To mimic the realistic observation network that has time-varying observing sites and dense temporal resolution, synthetic observations are taken every hour at a set of 50 locations that are randomly drawn from 5,000 nearly uniformly distributed locations on the sphere. To be consistent among the assimilation experiments, the same realization of random draws of observational locations is used for each assimilation experiment.

2.3. Data Assimilation and Initialization

To assimilate the synthetic observations, the serial ensemble square root filter (EnSRF; Whitaker & Hamill, 2002; Whitaker et al., 2008) is used here. Since the synthetic observations are available every hour, the ensemble observation priors are computed at the observation times, in order to avoid the time interpolation errors when assimilation windows are longer than 1 h. To mitigate spurious sample correlations and avoid filter divergence, covariance localization and covariance inflation are applied. Covariance localization that localizes the impact of observations on state variables as a function of the separation distance uses the Gaspari-Cohn (GC; Gaspari & Cohn, 1999) function. The GC localization function is an approximately Gaussian fifth-order piecewise continuous polynomial function, with a single parameter to define its width. Multiplicative covariance inflation, which inflates the posterior ensemble spread back to the prior ensemble spread proportional to the amount the ensemble spread is reduced by the assimilation of observations (Whitaker & Hamill, 2012), is used.

The analysis produced by intermittent DA with the EnKF may be dynamically inconsistent and contain unbalanced gravity waves that are absent in the real atmosphere due to the effects of sampling error and covariance localization (Lei, et al., 2012; Lie et al., 2012a, 2012b). One strategy to combat the imbalance is the incremental analysis update (IAU), which uses the dynamic model to gradually distribute the analyses increments over a time window. The traditional IAU often computes the analysis increment once at the middle of

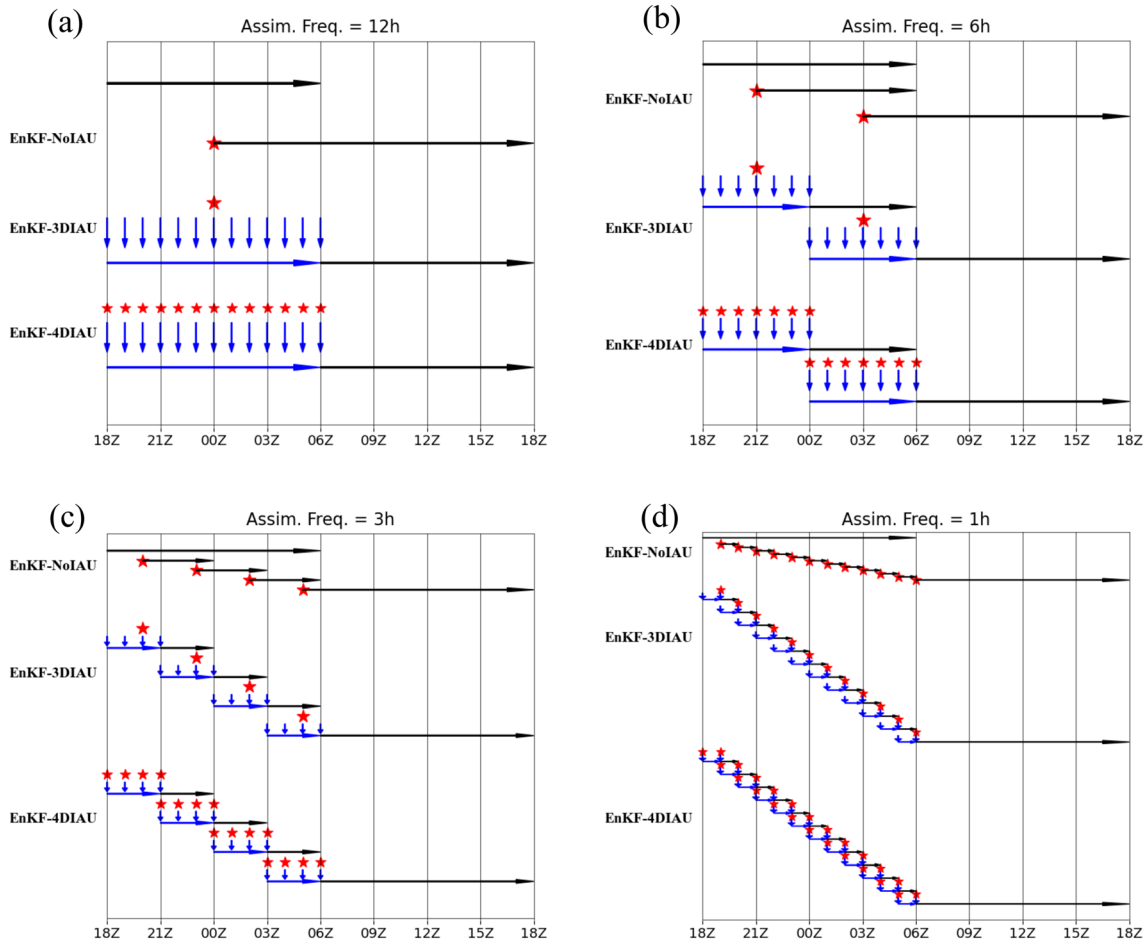

Figure 1. Schematic illustration of assimilation experiments with (a) 12-h, (b) 6-h, (c) 3-h, and (d) 1-h assimilation frequencies. Red stars denote analyses, perpendicular blue arrows display IAU increments and horizontal blue arrows show model integration with IAU, and horizontal black arrows denote free forecasts.

the assimilation window and assumes it to be constant over the assimilation window (Bloom et al., 1996), which can be seen as a three-dimensional IAU (3DIAU). To consider the propagation of the analysis increment in the assimilation window, Lei and Whitaker (2016) proposed a four-dimensional (4DIAU) that constructs time-varying analysis increments during the assimilation window and gradually applies these time-varying analysis increments through the assimilation window. Both 3DIAU and 4DAIU are used here based on the analysis increments obtained from the EnKF.

2.4. Experimental Design

Three groups of assimilation experiments are conducted: EnKF-NoIAU, EnKF-3DIAU, EnKF-4DIAU. All three experiments use EnKF to assimilate the synthetic observations. Experiment EnKF-NoIAU has no IAU forcing applied, while experiments EnKF-3DIAU and EnKF-4DIAU have 3DIAU and 4DIAU applied separately. Ensemble size is set to 20, and ensemble initial conditions are random draws from the model climatology.

Figure 1 displays a schematic of experiments with different assimilation frequencies. Given a 12-h assimilation frequency, experiment EnKF-NoIAU computes an analysis at the middle of the 12-h window given all observations in this 12-h window, and advances model till the end of next assimilation window. Similar to EnKF-NoIAU, experiment EnKF-3DIAU computes an analysis at the middle of the 12-h window, but it evenly distributes the increment (difference between analysis and forecast) along with model integration during the current 12-h assimilation window and continues to advance model without IAU forcing till the

Table 1
Optimally Tuned Assimilation Parameters for Each Assimilation Experiment With Different Assimilation Frequencies

Experiment	Assim. Freq.	Localization (km)	Inflation
EnKF-NoIAU	12	6,000	0.3
	6	10,000	0.3
	3	11,000	0.3
	1	13,000	0.3
EnKF-3DIAU	12	7,500 (9,000)	0.3 (0.3)
	6	10,000 (10,000)	0.3 (0.3)
	3	10,000 (11,000)	0.3 (0.3)
	1	10,000 (12,000)	0.3 (0.3)
EnKF-4DIAU	12	8,000 (9,000)	0.3 (0.3)
	6	10,000 (9,000)	0.3 (0.3)
	3	10,000 (10,000)	0.3 (0.3)
	1	12,000 (10,000)	0.3 (0.3)

Note. The values in parenthesis are for temporal weighting function of Lanczos.

end of next assimilation window. Experiment EnKF-4DIAU is similar to EnKF-3DIAU, except that it computes hourly analyses given all observations in this 12-h window and applies time-varying increments based on the hourly increments along with model integration during the current assimilation window. When assimilation frequency increases to 6, 3, and 1 h, the original 12-h assimilation window is divided to 2, 4, and 12 sub-assimilation windows. For each sub-assimilation window, the same assimilation procedures as the 12-h assimilation frequency are operated for experiments EnKF-NoIAU, EnKF-3DIAU, and EnKF-4DIAU, respectively. A 12-h forecast is launched at the end of each 12-h assimilation window. Thus, the same number of observations are assimilated with different assimilation frequencies, and the 12-h forecast launched at the end of each 12-h assimilation window can provide fair comparison for experiments with different assimilation frequencies.

To avoid the impact of increment frequency that is used to interpolate time-varying IAU forcing, experiments EnKF-4DIAU with different assimilation frequencies use the same increment frequency of 1 h. Since hourly model output is saved, analyses for 3-h (1-h) assimilation frequency are computed at 2 h (1 h) for each sub-assimilation window. The assimilation parameters, including the localization and multiplication inflation, are tuned to be optimal for each assimilation experiment separately, as shown in Table 1. For each assimilation experiment, a group of experiments with a range of localization and inflation values are performed, and the optimal localization and inflation are chosen when the minimal forecast errors are generally obtained. The default temporal weighting function for experiments EnKF-3DIAU and EnKF-4DIAU is a constant over the assimilation window, whose integral over the assimilation the window equals 1. Each assimilation experiment runs for 3,500 update cycles (each cycle with a 12-h assimilation window), and the last 2,000 cycles are used for verification.

To evaluate the results, the spectral coefficients of vorticity and divergence at two levels are transformed to u and v winds at two levels, and the layer thickness for each layer is transformed to surface and interface pseudo-height. The root-mean-square error (RMSE) relative to the nature run is computed for ensemble mean winds at each level, surface, and interface pseudo-height separately. The RMSE averaged over the 2,000 cycles is calculated. The sum of the layer thicknesses is the total mass, and the temporal evolution of the domain-averaged total mass tendency can be used as a measure of external mode gravity wave amplitude. Thus, this diagnostic as a noise parameter is used to measure the amplitude of imbalances introduced by the DA.

3. Two-Layer Model Results

The mean RMSEs in the current and next assimilation windows of experiments EnKF-NoIAU, EnKF-3DIAU, and EnKF-4DIAU with different assimilation frequencies are shown in Figures 2–4 separately, as a function of forecast hour. During current assimilation window ($-6 \ll t < 6$), experiment EnKF-NoIAU with 12-h assimilation frequency has an instantaneous error reduction at $t = 0$ h due to the insertion of analysis increments, and similarly experiments EnKF-NoIAU with 6- and 3-h assimilation frequencies have instantaneous error reductions at each insertion of analysis increment (Figure 2). Comparatively, experiments EnKF-3DIAU and EnKF-4DIAU with 12-h assimilation frequency have the error first decreasing and then increasing, with a minimum reached close to the middle of the assimilation window at $t = 0$ h (Figures 3 and 4). Similar error evolutions during each shorter assimilation window are obtained for experiments EnKF-3DIAU and EnKF-4DIAU with 6- and 3-h assimilation frequencies. This kind of error evolution during an assimilation window with IAU forcing indicates the trade-off between the forecast error growth and the inclusion of observation information via the IAU forcing (Lei & Whitaker, 2016). The instantaneous error reduction of EnKF-NoIAU and gradual error evolution of EnKF-3DIAU and EnKF-4DIAU during an assimilation window are not obvious for experiments with 1-h assimilation frequency since only hourly mean RMSE is shown.

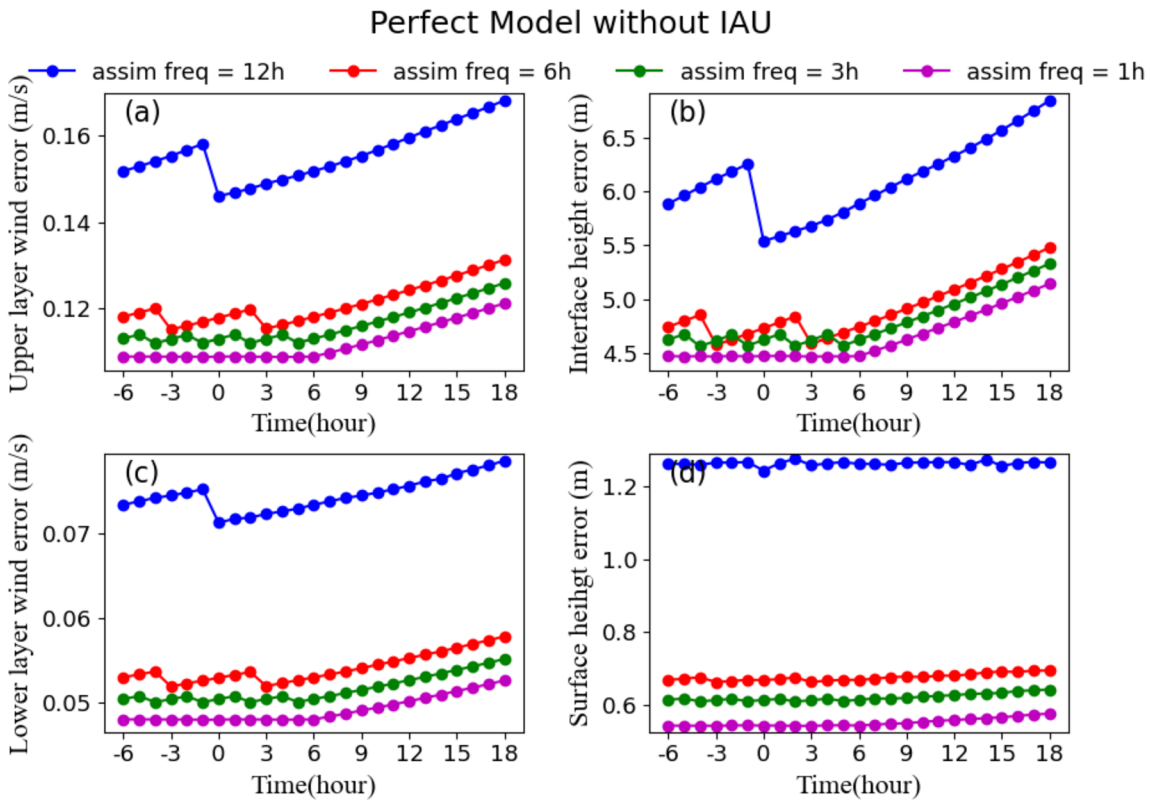

Figure 2. Mean RMSEs of experiment EnKF-NoIAU in the current (−6 to +6 h) and next (6 to 18 h) assimilation windows for (a) upper-level wind, (b) interface height, (c) lower-level wind, and (d) surface pseudo-height. These RMSEs are averaged over the last 2,000 cycles from a 3,500-cycle run, and each cycle has a 12-h assimilation window.

During the free forecast over the next assimilation window ($6 \ll t < 18$), increasing assimilation frequency of EnKF-NoIAU leads to decreased errors for all state variables, and the error reduction from 12- to 6-h assimilation frequency is most significant (Figure 2). EnKF-3DIAU with 6- and 3-h assimilation frequencies have smaller errors of upper layer wind and interface height than that with 12-h assimilation frequency, while EnKF-3DIAU with 1-h assimilation frequency further decreases the errors than that with 6- and 3-h assimilation frequencies (Figure 3). EnKF-3DIAU with 6-, 3-, and 1-h assimilation frequencies obtains similar errors of lower layer wind, which are much smaller than that with 12-h assimilation frequency. Since the surface pseudo-height (which is analogous to surface pressure) carries the signals of the external gravity mode, it is sensitive to the imbalance introduced by assimilation. EnKF-3DIAU with 6-h assimilation frequency has smaller errors than that with 12-h assimilation frequency, but further increasing assimilation frequency leads to increased errors for surface pseudo-height, especially for 1-h assimilation frequency. EnKF-4DIAU obtains similar results to EnKF-3DIAU. Increasing assimilation frequency of EnKF-4DIAU leads to decreased errors for upper layer wind and interface height (Figure 4). EnKF-4DIAU with 6- and 3-h assimilation frequencies has smaller errors of lower layer wind than that with 12-h assimilation frequency, while EnKF-4DIAU with 1-h assimilation frequency further decreases the errors than that with 6- and 3-h assimilation frequencies. EnKF-4DIAU with 6-h assimilation frequency has smaller errors of surface pseudo-height than that with 12-h assimilation frequency, but further increasing assimilation frequency leads to increased errors.

During the free forecast, the impacts of assimilation frequency of EnKF-NoIAU, EnKF-3DIAU, and EnKF-4DIAU on the surface pseudo-height are different from the other state variables, because the surface pseudo-height carries the signal of the external gravity mode and is sensitive to the imbalances introduced by assimilation. To quantitively measure the imbalances in the model states, the noise parameter that is the time mean domain-averaged absolute value of the total mass tendency is computed, shown by Table 2. EnKF-NoIAU, which has no IAU forcing, has decreased values of noise parameter when

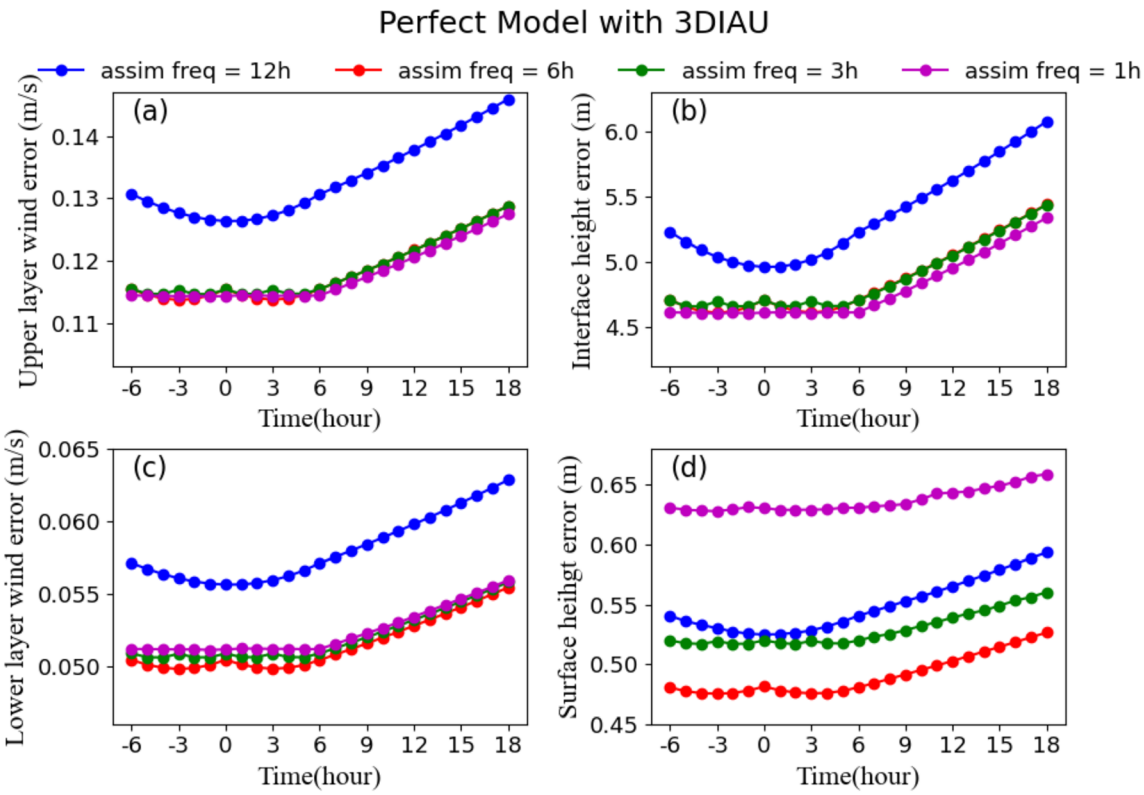

Figure 3. Same as Figure 2, except for experiment EnKF-3DIAU.

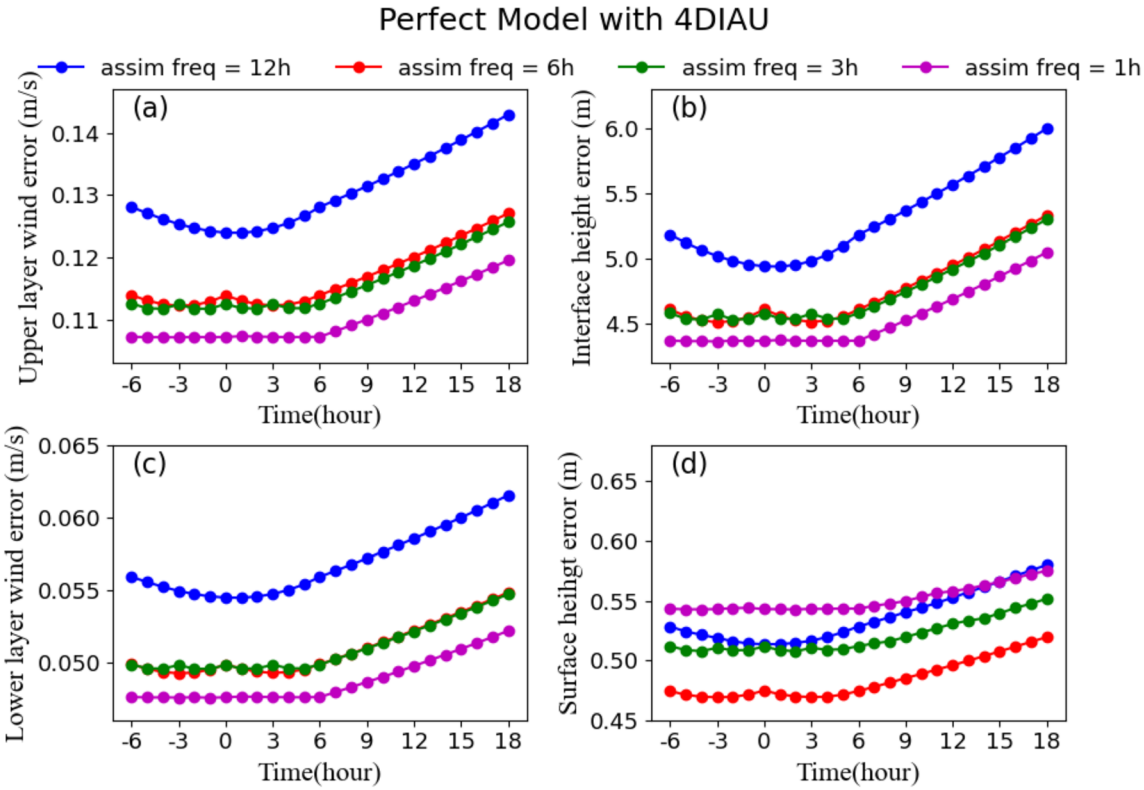

Figure 4. Same as Figure 2, except for experiment EnKF-4DIAU.

Table 2
Mean Noise Parameters ($\times 10^{-4}$ ms^{-1}) at the End of the Next Assimilation Window From Different Assimilation Experiments With Various Assimilation Frequencies

Assim. Freq.	EnKF-NoIAU	EnKF-3DIAU	EnKF-4DIAU
12	8.39	6.44 (6.44)	6.44 (6.44)
6	6.82	6.45 (6.46)	6.45 (6.65)
3	6.74	6.47 (6.53)	6.47 (6.56)
1	6.61	6.71 (6.61)	6.59 (6.74)

Note. The values in parenthesis are for temporal weighting function of Lanczos.

assimilation frequency increases. This is because more frequent assimilation can lead to less insertion noise caused by instantly update at each assimilation cycle. But EnKF-3DIAU and EnKF-4DIAU have increased values of noise parameter when assimilation frequency increases. Note that the minimum noise parameter of EnKF that is obtained with 1-h assimilation frequency is generally larger than those of EnKF-3DIAU and EnKF-4DIAU, which indicates that IAU can effectively reduce the imbalances (Lei & Whitaker, 2016).

By assimilating synthetic observations that are available every 12 h, Lei and Whitaker (2016) showed that EnKF-3DIAU and EnKF-4DIAU reduced imbalances in the analysis compared to EnKF-NoIAU, and EnKF-4DIAU outperformed EnKF-NoIAU and EnKF-3DIAU. Similar results are obtained here when synthetic observations are available every hour. Table 3 displays the mean RMSE at 12 h of the assimilation window for each experiment with different assimilation frequencies. When assimilation frequencies are 12 and 6 h, EnKF-4DIAU has slightly smaller errors than EnKF-3DIAU for all state variables. EnKF-4DIAU and EnKF-3DIAU produce smaller errors than EnKF-NoIAU, especially for the surface pseudo-height that carries the signals of the external gravity mode. When assimilation frequency increases to 3 and 1 h, EnKF-3DIAU generally has larger errors than EnKF-NoIAU, and EnKF-4DIAU obtains smaller errors than EnKF-NoIAU. Thus, with assimilation frequency varying from 12 to 1 h, EnKF-4DIAU produces better forecasts than either EnKF-NoIAU or EnKF-3DIAU for all state variables.

To examine the sensitivity of EnKF-3DIAU and EnKF-4DIAU with temporal weighting function, the Lanczos function (Takacs et al., 2018), which gives more weights to the middle of assimilation window and less weights to the beginning and end of assimilation window, is now used. Results of EnKF-3DIAU and EnKF-4DIAU with the Lanczos function are displayed in Figures 5 and 6, respectively. Compared to experiments EnKF-3DIAU and EnKF-4DIAU with a constant temporal weighting function (Figures 3 and 4), experiments EnKF-3DIAU and EnKF-4DIAU with 12-h assimilation frequency have error first increasing, and then decreasing to the minimum slightly later than the middle of the assimilation window (0 h), later increasing again, during current assimilation window. Experiments EnKF-3DIAU and EnKF-4DIAU with 6- and 3-h assimilation frequencies display similar error evolutions during the shorter assimilation windows. The error evolution is consistent with the temporal weighting function applied, which demonstrates the trade-off between the forecast error growth and the inclusion of observation information.

During the free forecast period, results obtained with the constant temporal weighting function are generally similar to those using the Lanczos function. EnKF-3DIAU has smaller errors of upper and lower layer winds and interface height with increasing assimilation frequency. EnKF-3DIAU with 6-h assimilation frequency has smaller errors of surface pseudo-height than that with 12-h assimilation frequency, but obtains larger errors with further increased assimilation frequencies. EnKF-4DIAU also obtains smaller errors of upper and lower layer winds and interface height with increasing assimilation frequency, especially for the

Table 3
Mean RMSEs at 12 h of the Assimilation Window for Experiments EnKF-NoIAU, EnKF-3DIAU, and EnKF-4DIAU With Different Assimilation Frequencies

Assim. Freq.	Exp. name	Upper layer wind (m/s)	Interface height (m)	Lower layer wind (m/s)	Surface height (m)
12 h	EnKF-NoIAU	0.1596	6.3277	0.0757	1.2645
	EnKF-3DIAU	0.1378	5.6273	0.0598	0.5652
	EnKF-4DIAU	0.1350	5.5679	0.0586	0.5526
6 h	EnKF-NoIAU	0.1242	5.0904	0.0553	0.6812
	EnKF-3DIAU	0.1217	5.0554	0.0528	0.5025
	EnKF-4DIAU	0.1201	4.9511	0.0522	0.4957
3 h	EnKF-NoIAU	0.1190	4.9569	0.0526	0.6278
	EnKF-3DIAU	0.1217	5.0526	0.0532	0.5390
	EnKF-4DIAU	0.1187	4.9219	0.0521	0.5307
1 h	EnKF-NoIAU	0.1146	4.7888	0.0501	0.5596
	EnKF-3DIAU	0.1206	4.9565	0.0534	0.6436
	EnKF-4DIAU	0.1130	4.6924	0.0497	0.5580

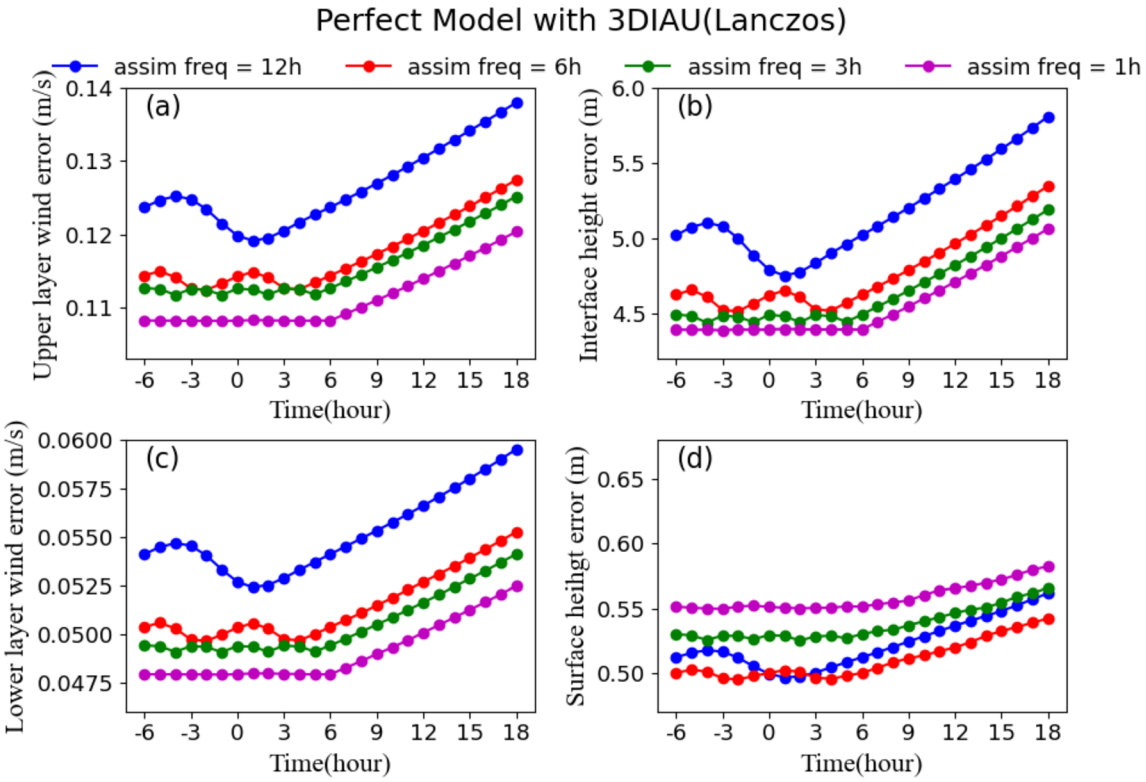

Figure 5. Same as Figure 3, except for temporal weighting function of Lanczos.

assimilation frequency increasing from 6 to 3 h. Comparatively, EnKF-4DIAU has larger errors of surface pseudo-height with increasing assimilation frequency. The noise parameters of EnKF-3DIAU and EnKF-4DIAU with Lanczos function are shown in Table 2. In general, EnKF-3DIAU and EnKF-4DIAU have increased values of noise parameter when assimilation frequency increases, which is consistent with the constant temporal weighting function.

Therefore, increasing assimilation frequency for EnKF-NoIAU, EnKF-3DIAU, and EnKF-4DIAU leads to smaller errors of upper and lower layer winds and interface height, which are less sensitive to the imbalances. But for surface pseudo-height that is sensitive to the imbalances, increasing assimilation frequency of EnKF-NoIAU produces smaller errors, since more frequent updates result in less insertion noise. When 3DIAU and 4DIAU with either the constant or Lanczos temporal weighting function are implemented, increasing assimilating frequency to 3 and 1 h results in larger errors of surface pseudo-height, which is also consistent with the noise diagnostic based on the global mass tendency.

4. Design of GFS Experiments

The potential advantages to improve global forecasts by increasing assimilation frequency are investigated in the NOAA GFS with real observations. The forecast model uses a dual-resolution configuration with a single control forecast at T670 and an 80-member ensemble at T25 resolution, with 64 vertical levels. In the dual-resolution experiments, the ensemble priors are first recentered around the control forecast at the beginning of each data assimilation cycle. The control and ensemble analyses are then computed separately, using all observations in the window. The control analysis is produced by the hybrid 4DEnVar algorithm (Kleist & Ide, 2015), and the ensemble analyses are produced by the EnKF (Whitaker & Hamill, 2002). The EnKF analyses are then recentered around the hybrid 4DEnVAR analysis. The control and ensemble analyses are at last advanced to the end of next data assimilation window.

Hybrid 4DEnVAR utilizes 4-D ensemble perturbations but a time-invariant static background error covariance (**B**) throughout the assimilation window. The amplitude of the time-invariant static **B** in the hybrid

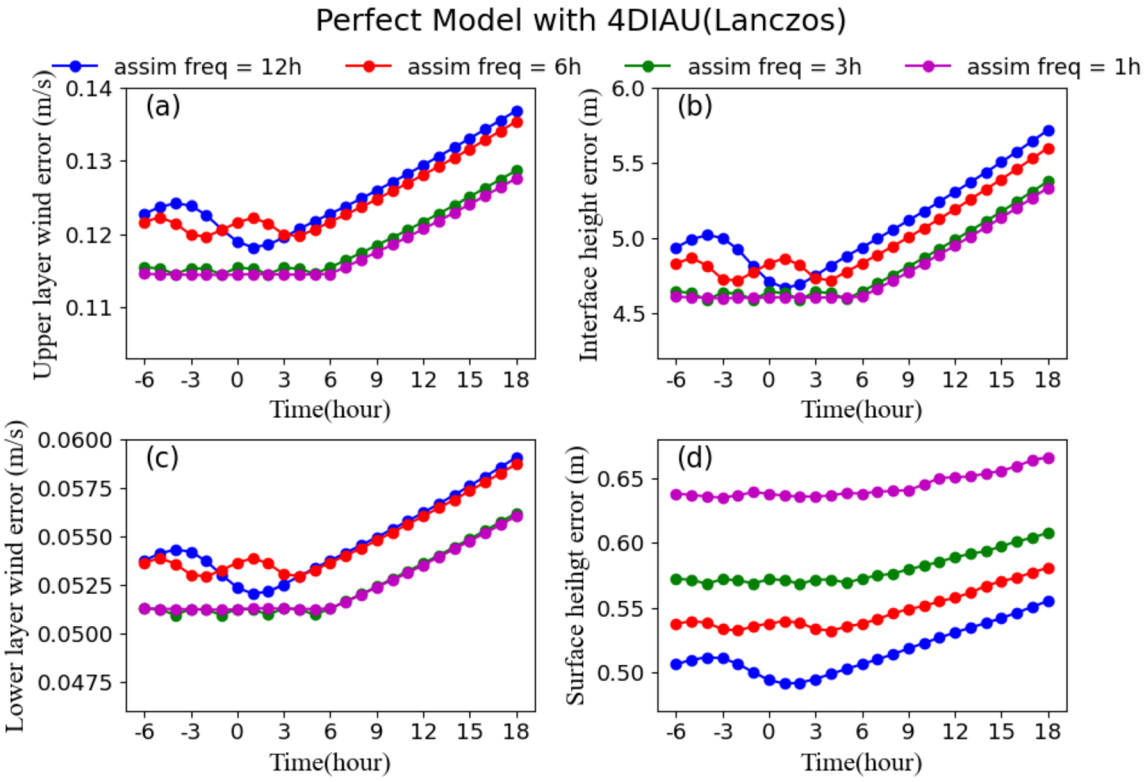

Figure 6. Same as Figure 4, except for temporal weighting function of Lanczos.

4DEnVAR is set to 0.125 that is the same as the value used in NOAA operations (Lei & Whitaker, 2017). To remove spurious long-range covariance arising from sampling errors, covariance localization is used. The localization is applied separately in the horizontal and vertical, and the same horizontal and vertical localization length scales are used in both hybrid 4DEnVAR and EnKF. Following Lei and Whitaker (2017), the level-dependent horizontal localization scale is used, and a constant vertical localization scale of 0.5 scale height is applied. To remedy the insufficient ensemble spread, multiplicative covariance inflation (Whitaker & Hamill, 2012) is used with the relaxation coefficient set to 0.85. Stochastic parameterizations (Palmer et al., 2009) are used to represent model uncertainty within the ensemble forecast step, and no additive inflation is applied.

All observations used operationally in the NOAA global data assimilation system (GDAS), including conventional in situ observations, and remotely sensed satellite radiances, cloud-motion vectors, and global positioning system radio-occultation measurements, are assimilated every 6 h. The observation error variances are the same as that used in the NOAA GDAS. To compute the observation prior ensemble $\mathbf{Hx}^b$ (needed by the EnKF) where $\mathbf{H}$ is the observation forward operator and $\mathbf{x}^b$ is the model ensemble background, the "observer" portion of the Grid-point Statistical Interpolation system (GSI) (Kleist et al., 2009; Wu et al., 2002) is run for the ensemble mean and each ensemble members separately.

The control experiment assimilates observations every 6 h, as the traditionally used assimilation frequency. To examine the impact of assimilation frequency, an additional experiment that assimilates observations every 2 h is conducted, with a 6-h forecast launched every 6 h to compare with the control. Both experiments are run from 00 UTC 1 April 2014 to 00 UTC 20 April 2014. The first 4 days of assimilation is discarded to avoid transient effects, and the remaining data are used for verification.

5. GFS Results

To evaluate the experiments, the globally and temporally averaged vertical profiles of the differences and RMS differences between the 6-h observation priors ($\mathbf{Hx}^b$) and in situ observations are shown in Figure 7.

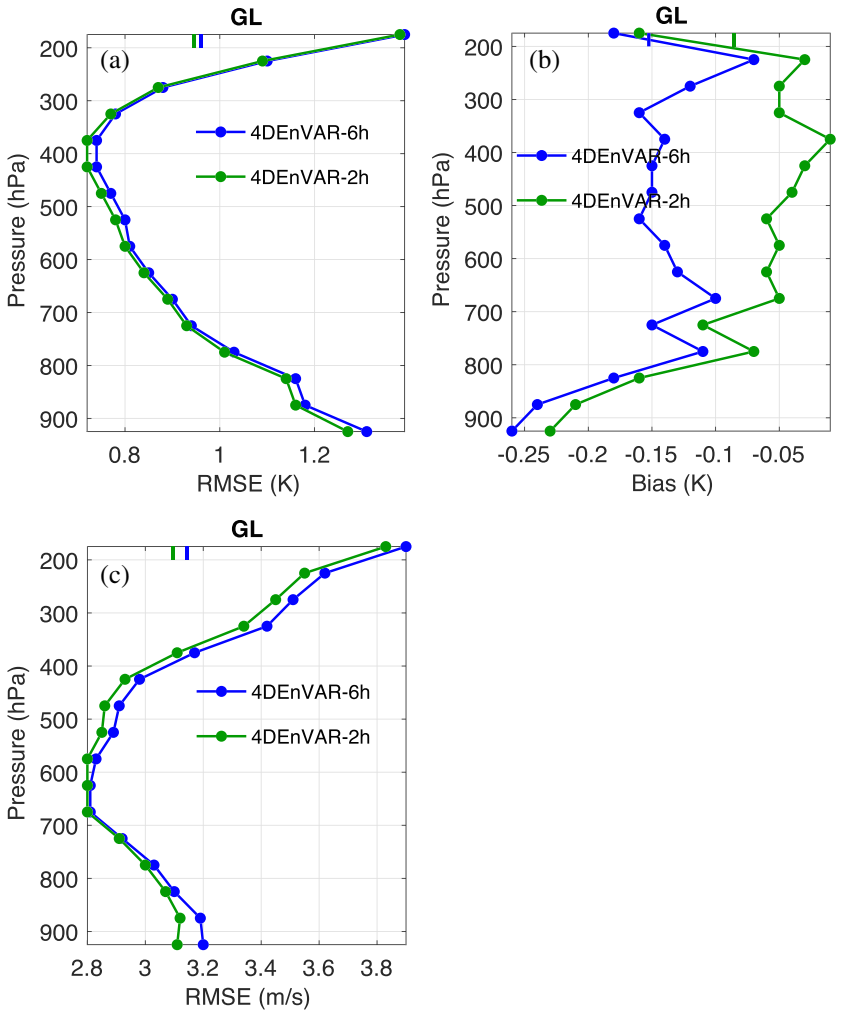

Figure 7. Globally and temporally averaged profiles of (a) temperature RMSE, (b) temperature bias, and (c) wind RMSE, which are computed from the 6-h forecasts verified relative to the conventional observations. The bars on top denote the mean values of the error and bias. These RMSEs are averaged from the verification period of 00 UTC 5 April 2014 to 00 UTC 20 April 2014.

The bars on top of each panel denote the mean values. Experiment 4DEnVAR-2h has smaller RMSE of temperature and wind speed than experiment 4DEnVAR-6h at nearly all vertical levels. Consistent results are also obtained for u- and v-winds separately (Figures are not shown). Moreover, experiment 4DEnVAR-2h produces much less bias of temperature than experiment 4DEnVAR-6h. Similar results are also obtained for the northern hemisphere, the tropics, and the southern hemisphere, respectively (figures are not shown).

Figure 8 displays the verification of the 6-h forecasts verified relative to the AMSU-A radiance observations. Channel 14 is not assimilated for all satellites that have AMSU-A onboard; thus, the errors of channel 14 is not shown. Experiment 4DEnVAR-2h has smaller RMSE than experiment 4DEnVAR-6h for channels 4–12, and it also produces much less biases than experiment 4DEnVAR-6h, especially for channels 4–12. Assimilation frequency has less impact on channels 1–3 and 15 than the other channels, possibly because channels 1–3 and 15 are sensitive to surface conditions and can be dominated by errors of observation forward operator and nonlinearity. Similar results are also obtained for the northern hemisphere, the tropics, and the southern hemisphere, respectively (figures are not shown).

The surface pressure tendency is a metric to measure the amount of imbalances generated by data assimilation (Lynch & Huang, 1992; Lei et al., 2012a). The surface pressure tendency between 3- and 0-h forecasts is

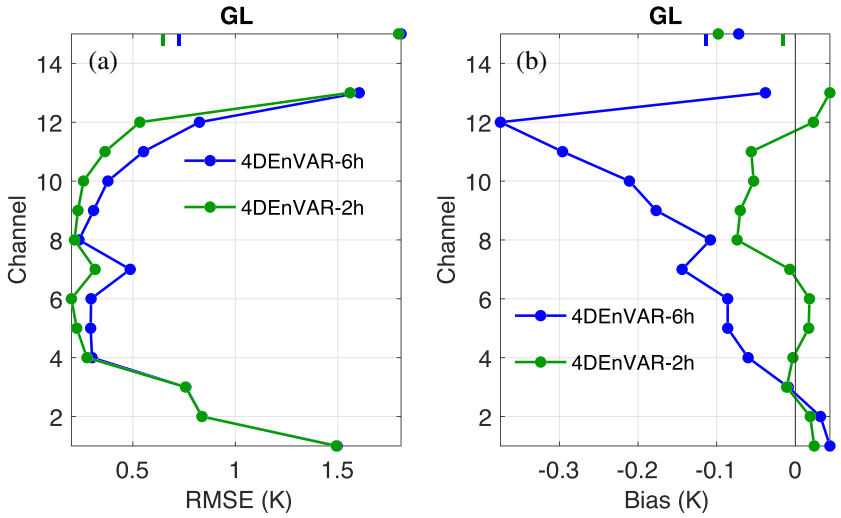

Figure 8. Globally and temporally averaged profiles of (a) RMSE and (b) bias for AMSU-A radiances, which are computed from the 6-h forecasts verified relative to the AMSU-A radiance observations. The bars on top denote the mean values of the error and bias.

averaged over the globe and the verification period. The globally and temporally averaged absolute 3-h surface pressure tendency of experiment 4DEnVAR-6h is 152.14 [hPa (3 h)$^{-1}$], and that of experiment 4DEnVAR-2h is 156.86 [hPa (3 h)$^{-1}$]. Experiment 4DEnVAR-2h has larger values of surface pressure tendency than experiment 4DEnVAR, indicating that more frequent assimilation lead to less balanced forecasts. This imbalance diagnostics is inconsistent with that in the two-layer model. One possible reason is the localization that can influence the imbalance of an EnKF (Greybush et al., 2011). The localization is optimally tuned for each experiment of the two-layer model with different assimilation frequencies. The optimal localization becomes broader when assimilation frequency increases (Table 1). But a fixed localization is used for GFS experiment with 6-h and 2-h assimilation frequencies. Given a fixed localization (7,000 km), experiment EnKF-NoIAU using the two-layer model has increased RMSEs of the surface pseudo-height (i.e., the imbalances) when assimilation frequency increases, which is consistent with the imbalances of GFS experiments (figures are not shown). Other possible reasons include the model errors that could have nonlinear interactions with smaller increments given more frequent assimilations and then exacerbate the imbalance and the moisture process presented in the real case simulation that might trigger more small-scale disturbances with more frequent updates and result in more imbalances.

Therefore, verifications based on both conventional and radiance observations show the advantages of increasing assimilation frequency from 6 h to 2 h for the NOAA GFS. Increasing the assimilation frequency can better combat the model bias, and then lead to improved forecasts, although result in less balanced forecasts reflected by larger values of surface pressure tendency.

6. Conclusions

The assimilation frequency has essential influences on the performances of data assimilation, especially for modern observation networks that have inhomogeneous observations in space and time. Thus, this study examines the impact of assimilation frequency on data assimilation and the imbalance caused by data insertion, using an idealized two-layer primitive-equation model and the NOAA GFS model.

Results from the idealized two-layer model show that EnKF-NoIAU, EnKF-3DIAU, and EnKF-4DIAU with increasing assimilation frequency have smaller errors of state variables that are not sensitive to imbalances, including the upper and lower layer winds and interface height. For state variable surface pseudo-height that is sensitive to imbalances, increasing assimilation frequency for EnKF-NoIAU that has no IAU forcing leads to reduced errors, because more frequent update results in less insertion noises. However, increasing

assimilation frequency for EnKF-3DIAU and EnKF-4DIAU that have initialization methods applied generally leads to increased errors. This is in agreement with the analysis of Lei and Whitaker (2016) and Bloom et al. (1996), which showed that the noise filtering properties of IAU are lessened as the length of the assimilation window decreases. The impact of assimilation frequency on EnKF-3DIAU and EnKF-4DIAU is consistent for both constant and Lanczos temporal weighting functions.

Using the realistic NOAA GFS model, increasing assimilation frequency from 6 to 2 h leads to improved 6-h forecasts of temperature and wind speed, especially for the reduced temperature bias. Moreover, increasing assimilation frequency from 6 to 2 h also improves the errors and biases of the AMSU-A radiance observations. The diagnostic of surface pressure tendency shows that, unlike in the two-layer model experiments without moist processes or model error, increasing assimilation frequency from 6 to 2 h results in less balanced forecasts, which may be due to a fixed localization value applied, and the model error and moisture process presented in real case simulations. Therefore, increasing assimilation frequency can lead to improved forecasts for variables insensitive to imbalances.

For the realistic GFS model, the influences of increasing assimilation frequency from 6 h to 2 h are examined here. But experiments that have more frequent assimilation than 2 h for realistic simulations need further studies. Moreover, the impact of increasing assimilation frequency on longer forecasts will be explored in future studies.

Data Availability Statement

The data used to generate the simulation experiments were obtained from the National Centers for Environmental Prediction (NCEP; https://www.ncdc.noaa.gov/data-access/model-data/model-datasets/global-forcast-system-gfs).

Acknowledgments
Thanks to two anonymous reviewers who helped to significantly improve the manuscript. This work is supported by the National Key Research and Development Program of China under Grants 2017YFC1501603 and the General Program of National Natural Science Foundation of China under Grants 41922036.

References

Aksoy, A., Dowell, D. C., & Snyder, C. (2009). A multicase comparative assessment of the ensemble Kalman filter for assimilation of radar observations. Part I: Storm-scale analyses. *Monthly Weather Review*, *137*(6), 1805–1824. https://doi.org/10.1175/2008MWR2691.1

Baer, F., & Tribbia, J. (1977). On complete filtering of gravity modes through non-linear initialization. *Monthly Weather Review*, *105*(12), 1536–1539. https://doi.org/10.1175/1520-0493(1977)105<1536:OCFOGM>2.0.CO;2

Bloom, S. C., Takacs, L. L., Da Silva, A. M., & Ledvina, D. (1996). Data assimilation using incremental analysis updates. *Monthly Weather Review*, *124*(6), 1256–1271. https://doi.org/10.1175/1520-0493(1996)124<1256:DAUIAU>2.0.CO;2

Buehner, M., Houtekamer, P. L., Charette, C., Mitchell, H. L., & He, B. (2010a). Intercomparison of variational data assimilation and the ensemble Kalman filter for global deterministic NWP. Part I: Description and single-observation experiments. *Monthly Weather Review*, *138*, 1550–1566.

Buehner, M., Houtekamer, P. L., Charette, C., Mitchell, H. L., & He, B. (2010b). Intercomparison of variational data assimilation and the ensemble Kalman filter for global deterministic NWP. Part II: One-month experiments with real observations. *Monthly Weather Review*, *138*(5), 1567–1586. https://doi.org/10.1175/2009MWR3158.1

Dong, J. L., & Xue, M. (2013). Assimilation of radial velocity and reflectivity data from coastal WSR-88D radars using an ensemble Kalman filter for the analysis and forecast of landfalling hurricane Ike (2008). *Quart. J. Roy. Meteor. Soc.*, *139*(671), 467–487. https://doi.org/10.1002/qj.1970

Gao, J., Xue, M., Brewster, K., & Droegemeier, K. K. (2004). A three-dimensional variational data analysis method with recursive filter for Doppler radars. *Journal of Atmospheric and Oceanic Technology*, *21*(3), 457–469. https://doi.org/10.1175/1520-0426(2004)021<0457:ATVDAM>2.0.CO;2

Gaspari, G., & Cohn, S. E. (1999). Construction of correlation functions in two and three dimensions. *Quart. J. Roy. Meteor. Soc.*, *125*(554), 723–757. https://doi.org/10.1002/qj.49712555417

Greybush, S. J., Kalnay, E., Miyoshi, T., Ide, K., & Hunt, B. R. (2011). Balance and ensemble Kalman filter localization techniques. *Monthly Weather Review*, *139*, 511–522.

Hamill, T. M., & Whitaker, J. S. (2005). Accounting for the error due to unresolved scales in ensemble data assimilation: A comparison of different approaches. *Monthly Weather Review*, *133*(11), 3132–3147. https://doi.org/10.1175/MWR3020.1

Honda, T., Miyoshi, T., Lien, G. Y., Nishizawa, S., Yoshida, R., Adachi, S. A., et al. (2018). Assimilating all-sky *Himawari-8* satellite infrared radiances: A case of Typhoon Soudelor (2015). *Monthly Weather Review*, *146*(1), 213–229. https://doi.org/10.1175/MWR-D-16-0357.1

Houtekamer, P. L., Deng, X., Mitchell, H. L., Baek, S., & Gagnon, N. (2014). Higher resolution in an operational ensemble Kalman filter. *Monthly Weather Review*, *142*(3), 1143–1162. https://doi.org/10.1175/MWR-D-13-00138.1

Houtekamer, P. L., & Mitchell, H. L. (2005). Ensemble Kalman filtering. *Quarterly Journal of the Royal Meteorological Society*, *131*(613), 3269–3289. https://doi.org/10.1256/qj.05.135

Hu, M., & Xue, M. (2007). Impact of configurations of rapid intermittent assimilation of WSR-88D radar data for the 8 May 2003 Oklahoma City tornadic thunderstorm case. *Monthly Weather Review*, *135*(2), 507–525. https://doi.org/10.1175/MWR3313.1

Huang, X.-Y., & Lynch, P. (1993). Diabatic digital-filtering initialization: Application to the HIRLAM model. *Monthly Weather Review*, *121*(2), 589–603. https://doi.org/10.1175/1520-0493(1993)121<0589:DDFIAT>2.0.CO;2

Johnson, A., Wang, X., Carley, J. R., Wicker, L. J., & Karstens, C. (2015). A comparison of multiscale GSI-based EnKF and 3DVar data assimilation using radar and conventional observations for midlatitude convective-scale precipitation forecasts. *Monthly Weather Review*, *143*(8), 3087–3108. https://doi.org/10.1175/MWR-D-14-00345.1

Johnson, A., & Wang, X. G. (2017). Design and implementation of a GSI-based convection-allowing ensemble data assimilation and forecast system for the PECAN field experiment. Part I: Optimal configurations for nocturnal convection prediction using retrospective cases. *Weather and Forecasting*, *32*, 289–315.

Kalnay, E. (2002). *Atmospheric Modeling* (p. 368). Data Assimilation and Predictability, Cambridge: Cambridge University Press.

Kleist, D. T., & Ide, K. (2015). An OSSE-based evaluation of hybrid variational-ensemble data assimilation for the NCEP GFS. Part II: 4DEn-VAR and hybrid variants. *Monthly Weather Review*, *143*(2), 452–470. https://doi.org/10.1175/MWR-D-13-00350.1

Kleist, D. T., Parrish, D. F., Derber, J. C., Treadon, R., Wu, W., & Lord, S. (2009). Introduction of the GSI into NCEP global data assimilation system. *Weather and Forecasting*, *24*(6), 1691–1705. https://doi.org/10.1175/2009WAF2222201.1

Lawson, L. M., Hofmann, E. E., & Spitz, Y. H. (1996). Times series sampling and data assimilation in a simple marine ecosystem model. *Deep Sea Research, Part II*, *43*(2-3), 625–651. https://doi.org/10.1016/0967-0645(95)00096-8

Lei, L., & Anderson, J. L. (2014). Impacts of frequent assimilation of surface pressure observations on atmospheric analyses. *Monthly Weather Review*, *142*, 4477–4483.

Lei, L., Stauffer, D. R., & Deng, A. (2012a). A hybrid nudging-ensemble Kalman filter approach to data assimilation. Part II: Application in a shallow-water model. *Tellus*, *64A*, 18,485.

Lei, L., Stauffer, D. R., & Deng, A. (2012b). A hybrid nudging-ensemble Kalman filter approach to data assimilation in WRF/DART. *Quarterly Journal of the Royal Meteorological Society*, *138*(669), 2066–2078. https://doi.org/10.1002/qj.1939

Lei, L., Stauffer, D. R., Haupt, S. E., & Young, G. S. (2012). A hybrid nudging-ensemble Kalman filter approach to data assimilation. Part I: Application in the Lorenz system. *Tellus*, *64A*, 18,484.

Lei, L., & Whitaker, J. S. (2016). A four-dimensional incremental analysis update for the ensemble Kalman filter. *Monthly Weather Review*, *144*(7), 2605–2621. https://doi.org/10.1175/MWR-D-15-0246.1

Lei, L., & Whitaker, J. S. (2017). Evaluating the trade-offs between ensemble size and ensemble resolution. *Journal of Advances in Modeling Earth Systems*, *9*, 781–789. https://doi.org/10.1002/2016MS000864

Lynch, P., & Huang, X.-Y. (1992). Initialization of the HIRLAM model using a digital filter. *Monthly Weather Review*, *120*(6), 1019–1034. https://doi.org/10.1175/1520-0493(1992)120<1019:IOTHMU>2.0.CO;2

Machenhauer, B. (1977). On the dynamics of gravity oscillations in a shallow water model with applications to normal mode initialization. *Contributions to Atmospheric Physics*, *50*, 253–271.

Palmer, T. N., Buizza, R., Doblas-Reyes, F., Jung, T., Leutbecher, M., Shutts, G. J., et al. (2009). Stochastic parameterization and model uncertainty. ECMWF Tech. Memo. 598, 44 pp., Eur. Cent. for Medium-Range Weather Forecasts, Reading, U. K. [Available at http://www.ecmwf.int/sites/default/files/elibrary/2009/11577-stochastic-parametrization-and-model-uncertainty.pdf.]

Pan, Y. J., & Wang, M. J. (2019). Impact of the assimilation frequency of radar data with the ARPS 3DVar and cloud analysis system on forecasts of a squall line in southern China. *Advances in Atmospheric Sciences*, *36*(2), 160–172. https://doi.org/10.1007/s00376-018-8087-5

Penny, S. G., Bach, E., Bhargava, K., Chang, C.-C., Da, C., Sun, L., & Yoshida, T. (2019). Strongly coupled data assimilation in multiscale media: Experiments using a quasi-geostrophic coupled model. *Journal of Advances in Modeling Earth Systems*, *11*, 1803–1829. https://doi.org/10.1029/2019MS001652

Snyder, C., & Zhang, F. (2003). Assimilation of simulated Doppler radar observations with an ensemble Kalman filter. *Monthly Weather Review*, *131*(8), 1663–1677. https://doi.org/10.1175//2555.1

Takacs, L., Suarez, M., & Todling, R. (2018). The stability of incremental analysis update. *Monthly Weather Review*, *146*(10), 3259–3275. https://doi.org/10.1175/MWR-D-18-0117.1

Valdes-Abellan, J., Pachepsky, Y., Martinez, G., & Pla, C. (2019). How critical is the assimilation frequency of water content measurements for obtaining soil hydraulic parameters with data assimilation? *Vadose Zone Journal*, *18*(1), 1–10. https://doi.org/10.2136/vzj2018.07.0142

Wang, S., Xue, M., & Min, J. (2013). A four-dimensional asynchronous ensemble square-root filter (4Den SRF) algorithm and tests with simulated radar data. *Quarterly Journal of the Royal Meteorological Society*, *139*(672), 805–819. https://doi.org/10.1002/qj.1987

Whitaker, J. S., & Hamill, T. M. (2002). Ensemble data assimilation without perturbed observations. *Monthly Weather Review*, *130*(7), 1913–1924. https://doi.org/10.1175/1520-0493(2002)130<1913:EDAWPO>2.0.CO;2

Whitaker, J. S., & Hamill, T. M. (2012). Evaluating methods to account for system errors in ensemble data assimilation. *Monthly Weather Review*, *140*(9), 3078–3089. https://doi.org/10.1175/MWR-D-11-00276.1

Whitaker, J. S., Hamill, T. M., Wei, X., Song, Y., & Toth, Z. (2008). Ensemble data assimilation with the NCEP Global Forecast System. *Monthly Weather Review*, *136*(2), 463–482. https://doi.org/10.1175/2007MWR2018.1

Wu, W. S., Purser, R. J., & Parrish, D. F. (2002). Three-dimensional variational analysis with spatially inhomogeneous covariances. *Monthly Weather Review*, *130*, 2905–2916.

Zou, X., Barcilon, A., Navon, I. M., Whitaker, J., & Cacuci, D. G. (1993). An adjoint sensitivity study of blocking in a two-layer isentropic model. *Monthly Weather Review*, *121*(10), 2833–2857. https://doi.org/10.1175/1520-0493(1993)121<2833:AASSOB>2.0.CO;2